Polymer Chemistry

ROYAL SOCIETY OF CHEMISTRY

PAPER

View Article Online
View Journal

Cite this: DOI: 10.1039/d6py00098c

Pyrrolidinium-based gel composites for reprocessable, flame-retardant electrolytes

Haobo Hong,†[a] Tshepiso L. Tema,†[a,b] Redoy Gazi Shuvo,[a] Harald Rupp,[c] Stephanie Krüger,[d] Anja Marinow,*[a] Zviadi Katcharava*[a,b] and Wolfgang H. Binder*[a,b]

Received 29th January 2026,
Accepted 11th May 2026

DOI: 10.1039/d6py00098c

rsc.li/polymers

Flame-retardant and reprocessable gel composites composed of a pyrrolidinium-based poly(ionic liquid) were successfully prepared by incorporating surface-modified SiO_2-nanoparticles functionalized with ionic liquids or multiple hydrogen bonding groups (ureidopyrimidinones). Covalent functionalization was verified by CP-MAS ^{29}Si NMR, FT-IR, and thermogravimetric analysis. Surface-modified NPs significantly improved the dynamic characteristics of the synthesized gel composites, yielding composites with enhanced reprocessability and remarkable mechanical flexibility, reaching an elongation at break of up to 460%, achieved solely through reversible dynamic interactions without the need for permanent covalent crosslinking. Upon reprocessing, the ionic conductivity of the gels was efficiently restored, reaching values of 2.2×10^{-4} S cm^{-1} at room temperature. The composites further exhibited excellent thermal stability up to 330 °C and an inherently flame-retardant nature classified as UL 94 V-0 grade. These combined features underscore the potential of the developed PIL-based gel composites for safe, durable, and high-performance applications in electrochemical and flexible devices.

Introduction

Lithium-ion batteries (LIBs) have become an indispensable part of modern life. Major progress has been made in improving their performance, durability, and efficiency over the past few decades.[1,2] However, safety remains a persistent concern linked to the organic solvent-based electrolytes used in most commercial batteries. The flammability of these electrolytes can pose serious fire hazards, especially when exposed to mechanical/thermal/electrical misuse or when lithium dendrites form during cycling, which can trigger thermal runaway.[3] Material recyclability/reprocessability is another critical factor, particularly as global reliance on energy storage devices is rapidly increasing.[4,5] Researchers have been developing alternative electrolyte materials that can resolve reprocessability/recyclability concerns and safety aspects while maintaining or even enhancing performance.[6,7] Ionic liquids (ILs) and poly(ionic liquid)s (PILs) in particular have emerged as promising candidates.[8,9] They offer wide electrochemical stability windows, good ionic conductivity, and inherent non-flammability. Converting these liquid electrolytes into solid or gel-like materials opens new opportunities for advanced energy-storage systems, including flexible and reprocessable energy storage designs.[10–12] PILs combine the structural advantages of polymers with the ionic conductivity of ILs. They are particularly appealing because they can form stable, solvent-free electrolytes with excellent thermal and electrochemical properties.[13,14] In addition, their tunable chemical structure allows for fine adjustment of mechanical strength, ion transport pathways, and interfacial compatibility with electrodes. However, PILs are still limited in practical use due to their lower conductivity than that of liquid electrolytes. Embedding dynamic bonds into these materials is an attractive strategy to significantly enhance performance and material properties. These reversible covalent or non-covalent interactions can break and reform under external stimuli, enabling self-healing, recycling, and reprocessing. Dynamic covalent exchange chemistries, such as boronic esters, imines, and disulfide are commonly used for generating vitrimeric electrolytes, where choice of the proper bond controls dynamic properties, activation energy, reprocessing conditions, and self-

[a]Macromolecular Chemistry, Division of Technical and Macromolecular Chemistry, Faculty of Natural Sciences II (Chemistry, Physics, Mathematics), Institute of Chemistry, Martin Luther University Halle-Wittenberg, von-Danckelmann-Platz 4, D-06120 Halle, Germany. E-mail: anja.marinow@chemie.uni-halle.de, zviadi.katcharava@chemie.uni-halle.de
[b]Design of 3D-Printable Polymers Based on Regional Resources, Just Transition Center, Martin-Luther-University of Halle-Wittenberg University, 06099 Halle, Germany
[c]Institut für Kunststofftechnologie und -recycling e.V., 06369 Weißandt-Gölzau, Germany
[d]Biocenter, Microscopy Unit, Martin Luther University Halle-Wittenberg, Weinbergweg 22, 06120 Halle/Saale, Germany
† H. H. and T. L. T. contributed equally to this work.

healing efficiency.[15–17] Supramolecular interactions in polymer networks promote self-healing and reprocessability, with hydrogen bonds being among the most studied and successfully exploited ones.[6,18] In parallel, nanofillers represent another effective way to boost the properties of electrolytes, especially in terms of conductivity and mechanical strength. Inorganic fillers such as aluminum oxide (Al_2O_3), silica (SiO_2), and titanium oxide (TiO_2) have been widely incorporated into polymer matrices like polyethylene oxide (PEO) to form polymer composite electrolytes.[19–21] Surface modification of these nanoparticles can further improve their dispersivity and strengthen their interactions within a polymer network, leading to improved conductivity and mechanical properties.[22–24]

In this study, we report the development of flame-retardant, stretchable, reprocessable, and conductive materials based on dynamic poly(ionic liquid) network composites. Gel polymer electrolytes require reprocessability not only from the perspective of sustainability, but also to enhance the lifetime and economic features of advanced battery systems. In addition, during battery manufacturing, processing defects such as incomplete wetting, film imperfections, or inhomogeneous thickness may occur. Reprocessable gel electrolytes therefore allow the correction of defects without complete disposal of the material, thereby significantly improving manufacturing efficiency. Our design strategy here is centered around silica nanoparticles whose surfaces were modified with two different functional groups to impart compatibility with the surrounding matrix and allow for dynamic properties inside the electrolyte. Firstly, ureidopyrimidinone (UPy), which forms strong and reversible quadruple hydrogen bonds, was embedded to create dynamic crosslinks and enhance mechanical properties;[25–27] secondly we used modified ionic liquid moieties to improve nanoparticle dispersibility and promote ionic interactions throughout the polymer network.[24,28–30]

Our approach focuses on formulating PIL gels and composites that combine safety, flexibility, and high ionic conductivity. Pyrrolidinium-based ionic liquids and the corresponding monomers were chosen due to their outstanding electrochemical and thermal stability.[31] The influence of silica nanofillers with different surface chemistries on the structural and electrochemical behavior of the gels was systematically explored. A schematic overview of the designed gel structure is shown in Fig. 1, illustrating the main components: a pyrrolidinium-based acrylate monomer that polymerizes to form the PIL backbone; a UPy monomer, integrated into the polymer network to introduce reversible supramolecular interactions that enhance reprocessability and mechanical resilience; a mobile ionic phase, consisting of a pyrrolidinium-based ionic liquid (PMPyrr TFSI) and lithium salt (LiTFSI), providing the primary ionic conduction pathway; surface-modified silica nanofillers, acting as a reinforcing agent promoting dynamic crosslinking and high stretchability; and a photoinitiator to enable UV-curing during material fabrication.

This work aims to establish a versatile design concept for multicomponent PIL-based composite gels that unite safety, flexibility, and high ionic mobility.

Experimental

Materials and instrumentation

All chemicals were used as received from Sigma Aldrich, TCI, Alfa Aesar, abcr and Io-li-tec unless otherwise stated. DCM and chloroform were dried by refluxing over calcium hydride prior to use. Dry DMF and ACN were collected from the solvent purification system (mBraun SPS5).

Cross-polarization (CP) magic-angle spinning (MAS) solid-state NMR spectra of ^{29}Si were recorded at ambient temperature on a Bruker Avance II 400 spectrometer, equipped with a 4 mm MAS probe, with an MAS of 5 kHz, a CP time of 10 ms and a repetition delay of 5 s.

Thermogravimetric analysis (TGA) was conducted on a Netzsch TG 209 F3. Samples (5–15 mg) were placed in alumina crucibles and heated from 35 °C to 800 °C at a heating rate of 10 K min^{-1} under a nitrogen atmosphere (flow rate: 20 mL min^{-1}). The NETZSCH Proteus was used for analyzing the recorded data.

Fourier-transform infrared spectroscopy (FT-IR) analysis was conducted using the attenuated total reflection technique on a VERTEX 70v FT-IR spectrometer (Bruker) equipped with the Golden Gate diamond ATR unit. Measurements were conducted at room temperature in the spectral range of 550–4000 cm^{-1}.

Dynamic light scattering (DLS) analysis was performed using a Litesizer 500 (Anton Paar) equipped with a 40 mW single-frequency laser diode (at a wavelength of 658 nm). All data were processed using Kalliope software.

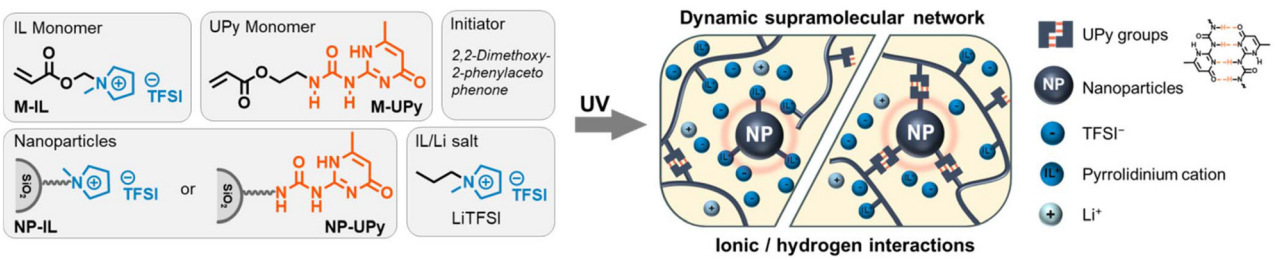

Fig. 1 Gel components and schematic representation of gel composites.

Negative-stain TEM grid preparation and imaging. Continuous carbon copper grids (200 mesh; Formvar-supported) were glow-discharged (Pelco easyGlow; 30 s; air; standard settings). Subsequently, 3 μL of sample was applied to each grid and incubated for 1 min. Excess liquid was removed by side blotting with filter paper. Then, the grids were washed by floating them on drops of distilled water three times for 1 min each. For negative staining, grids were floated on a drop of 2% (w/v) aqueous uranyl acetate for 1 min and side blotted. For each sample, grids were prepared with uranyl acetate staining and without stain (omitting the uranyl acetate step after the water washes) to control for staining artefacts. Prepared grids were stored in grid boxes until imaging. Images were acquired on a Zeiss EM900 transmission electron microscope operated at 80 kV using a 1k slow scan CCD camera (TRS Restlichverstärkersysteme).

Tensile tests were conducted using an INSTRON 5900 Series universal testing system machine. Dumbbell samples (ISO 37 Type 2) were produced using a pneumatic cutter (P-VS 3000, MonTech Rubber Testing Solutions). Measurements were performed at room temperature at a strain rate of 20 mm min^{-1}. Data analysis was performed *via* Bluehill Universal (version 4.08).

Broadband dielectric spectroscopy (BDS) was used for investigating ionic conductivities on a Novocontrol "Alpha analyzer". PIL gels were placed between two brass electrodes (d = 20 mm), and the thickness of each sample gel was measured individually (sample thickness ranged from 0.20 mm to 0.50 mm). The measuring cell was placed in a cryostat with a constant flow of dry nitrogen. Ionic conductivity was recorded in the frequency range of 1–10^6 Hz and at different temperatures. Ion conductivity values were extracted from the plateau of σ *vs.* T.

Reprocessing of gel composites was done using a vacuum compression molding (VCM) tool from MeltPrep. The sample was placed in the VCM disc tool with a diameter of 20 mm and heated at 120 °C for 3 hours. Subsequently, the tool was placed in the cooling unit and the restored sample was removed.

Synthesis

1-(3-(Acryloyloxy)propyl)-1-methylpyrrolidin-1-ium bis (trifluoromethylsulfonyl)amide (**M-IL**) and 2-(3-(6-methyl-4-oxo-1,4-dihydropyrimidin-2-yl)ureido)ethyl acrylate (**M-UPy**) were synthesized using a three-step reaction reported previously.[32,33] The corresponding procedures are described in detail in the SI, together with the full characterization data (for NMR spectra, see Fig. S1–S7).

Surface modification of nanoparticles

Surface modification of NPs was done according to Scheme 1. **NP-UPy** was prepared in a two-step reaction: in the first step, 3 g of Ludox® SM solution was diluted with deionized water to 100 mL. The mixture was kept for stirring and heated to 80 °C, followed by the gradual addition of 0.9 g (5 mmol) of 3-(trimethoxysilyl)propan-1-amine *via* a syringe. The reaction was maintained under continuous stirring at 80 °C for 48 h. Upon

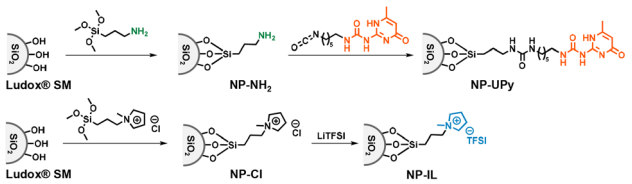

Scheme 1 Surface modification of Ludox® SM with IL and UPy groups.

completion, the resulting dispersion was concentrated using a rotavapor. The concentrated colloid was then precipitated in acetone. The obtained **NP-NH_2** was separated from the solvent using a centrifuge, washed 3 times using acetone and subsequently dried in an oven at 60 °C under vacuum.

In the second step, 1 g of **NP-NH_2** (1 g) was dispersed in dry $CHCl_3$ (100 mL), and subsequently, 1-(6-isocyanatohexyl)-3-(4-methyl-6-oxo-1,6-dihydropyrimidin-2-yl)urea (**UPy-NCO**) (0.62 g, 2.1 mmol, previously synthesized according to the literature[34]) was added. The reaction was refluxed under an inert atmosphere for 24 h. The modified particles were washed with $CHCl_3$ for removing unreacted (6-isocyanatohexyl)-3-(4-methyl-6-oxo-1,6-dihydropyrimidin-2-yl)urea. **NP-UPy** was collected by centrifugation and dried in an oven at 60 °C under vacuum (1.2 g of product obtained).

NP-IL was prepared by a previously described procedure.[29] Initially, *N*-[3-(trimethoxy silyl)propyl]-*N*-methylpyrrolidinium chloride was prepared with the following procedure: a mixture of *N*-methylpyrrolidinium (5 mL, 47 mmol) and (3-chloropropyl)trimethoxysilane (8.57 mL, 47 mmol) was kept at 80 °C while stirring for 48 hours under an inert atmosphere. The red/orangish mixture was washed using diethyl ether (4 times), and the obtained product was dried in a vacuum. The yield was 45%. ^{1}H NMR ($CDCl_3$, 400 MHz, δ in ppm): 3.78–3.61 (m, 4H), 3.54–3.47 (m, 2H), 3.45 (s, 9H), 3.19 (s, 3H), 2.27–2.08 (m, 4H), 1.80–1.68 (m, 2H), 0.61–0.53 (m, 2H). ^{13}C NMR ($CDCl_3$, 101 MHz, δ in ppm): 65.36, 64.15, 50.62, 48.40, 21.5, 17.59, 5.77.

A Ludox-sm® silica nanoparticle solution (3 g) was diluted with deionized water (100 g), and 0.7 g (2.5 mmol) of *N*-[3-(trimethoxysilyl)propyl]-*N*-methylpyrrolidinium chloride was added to the solution. The mixture was stirred continuously at 80 °C for 24 hours. Modified nanoparticles were concentrated using a rotary evaporator and precipitated into acetone. **NP-Cl** was collected using centrifugation and washed with acetone three more times. Subsequently, **NP-CL** (4.5 g) was dissolved in 120 mL of deionized water and mixed with 20 mL of a solution containing 4 g (14 mmol) LiTFSI. The mixture was kept for stirring for 8 hours at room temperature, after which the final product was collected *via* centrifugation and washed with deionized water (4 times). **NP-IL** was dried under vacuum at 70 °C for 24 hours.

PIL gel composite preparation.[32] In a typical gel preparation procedure, initiator (DMPA), **M-IL**, **M-UPy** and modified nanofillers (**NP-IL** or **NP-UPy**) were weighed in a dried vial equipped with a magnetic stirring bar. The ionic liquid (PMPyrr TFSI)

and lithium salts (LiTFSI) were added into the vial in the glovebox. The vial was taken out of the glovebox and dry DCM was rapidly added as the solvent and the vial was sealed with a screw cap. The mixture was stirred till the solid part was totally dissolved. The mixture was then quickly transferred to a one-neck flask, and the DCM was removed using a rotavapor at RT under vacuum. The gel precursor was transferred into a glovebox, spread evenly on a Petri dish and polymerized under UV light (λ = 365 nm) for 1 h. The final polymerized film was removed from the Petri dish carefully and cut into different specimens in a glovebox for the subsequent characterization studies.

Results and discussion

Surface modification of nanoparticles

To prepare the gel composites, the initial step involved modification of commercially available silica nanoparticles (Ludox® SM) for introducing ionic liquid groups or supramolecular moieties (UPy) on the surface. Following the modification and purification procedures described in the Experimental section, the obtained NPs (Fig. 2A) were thoroughly characterized by ^{29}Si CP-MAS NMR, TGA, and FT-IR spectroscopy. Fig. 2B shows the ^{29}Si CP-MAS spectra before and after surface modification. The appearance of new peaks at −68 and −58 ppm indicates the covalent attachment of organic moieties to the silica surface. According to conventional nomenclature, these peaks correspond to T_3 ($RSi(O_{0.5})_3$) and T_2 ($RSi(O_{0.5})_3$), where R represents the covalently attached organic group.[35–37] The higher intensity of the T_3 signal suggests that most surface species are bound through three siloxane linkages to the nanoparticle surface.

Additionally, the decrease in the Q_3 peak intensity (around −100 ppm) after modification indicates a reduction in the number of silanol groups, which is consistent with successful covalent functionalization of the silica nanoparticles. Fig. 2C shows the IR spectra of the nanoparticles, highlighting the appearance of alkyl C–H stretching vibrations (2800–3000 cm^{-1}) after surface modification. **NP-IL** exhibits characteristic bands of the $TFSI^-$ counterion at 1349 cm^{-1} (SO_2 stretching) and 1179 cm^{-1} (CF_3 stretching).[38,39] On the other hand, **NP-UPy** shows new bands in the 1400–1700 cm^{-1} region, corresponding to C═O, C–N, and N–H bond vibrations, confirming successful functionalization.[40–42] Thermogravimetric analysis was employed to quantify the degree of surface modification (Fig. 2D), assuming that the observed weight loss primarily arises from the degradation of the organic surface layer, while contributions from moisture evaporation and dihydroxylation are negligible. The TGA thermograms (Fig. 2D) display the mass loss of Ludox-sm®, **NP-NH$_2$**, **NP-UPy**, and **NP-IL**. Based on these values, the concentration of ionic liquid functional groups in **NP-IL** was calculated to be 0.81 mmol g^{-1}, while **NP-UPy** exhibited functional group concentrations of 0.68 mmol g^{-1}. Ludox SM is reported to have a specific surface area of 320–400 m^2 g^{-1}. According to the literature, the surface silanol density can be approximated as 5 OH per nm^2,[43] thereby estimating the total number of hydroxyl groups of Ludox SM to be (1.6–2.0) × 10^{21} OH per gram, corresponding to 2.66–3.32 mmol g^{-1}. Since we cannot exactly assess the fractions of the bi-(T_2) or tri-(T_3) siloxane linkages, the precise extent of the surface modification is difficult to determine. Assuming that attachment sites with T_3 predominate, the estimated extent of surface modification is 85–91% for **NP-IL** and 61–77% for **NP-UPy**.

The size of the nanoparticles was monitored throughout the modification process to ensure that the particles remained

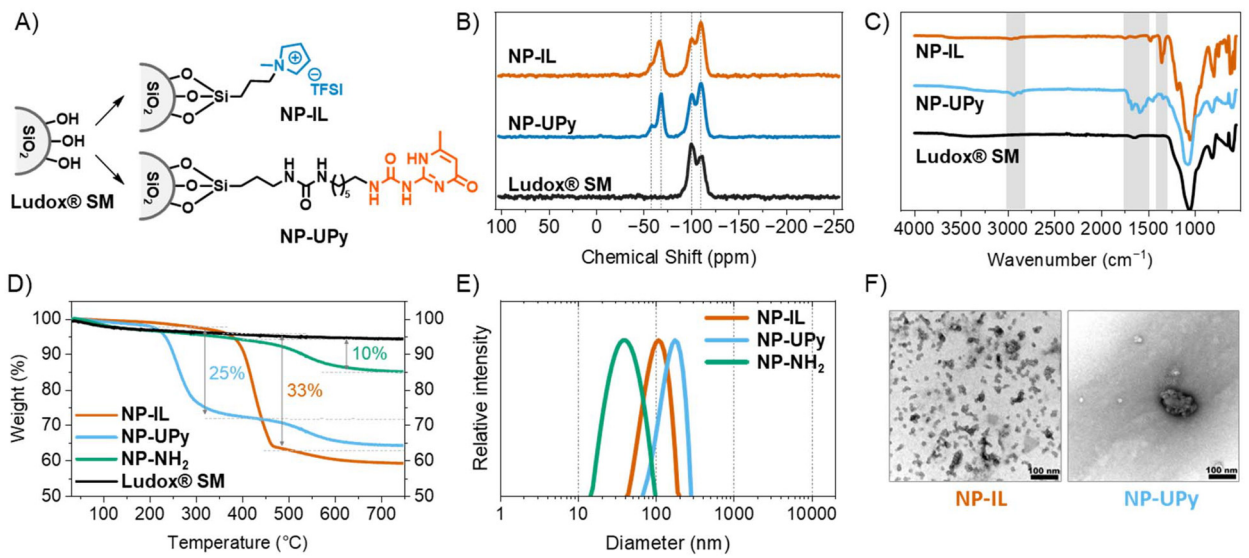

Fig. 2 (A) Chemical structure of surface-modified NPs, (B) Si^{29} CP MAS solid-state NMR, (C) FT-IR spectra of surface modified nanoparticles, (D) thermogravimetric analysis, (E) size distribution of surface-modified NPs and (F) corresponding TEM images.

within the expected range. The starting material (Ludox® SM) with an average particle diameter of 7 nm exhibited a gradual increase in size after each functionalization step. **NP-NH$_2$** showed the smallest average diameter, followed by **NP-IL** and **NP-UPy**. Dynamic light scattering (Fig. 2E) analysis indicated that **NP-UPy** exhibited a hydrodynamic diameter exceeding 100 nm, which is attributed to supramolecular aggregation driven by the strong UPy–UPy interactions. This clustering behavior was further verified by transmission electron microscopy (Fig. 2F), which showed the presence of aggregated domains. In contrast, **NP-IL** exhibited a smaller hydrodynamic radius, consistent with the TEM observations of well-dispersed particles and reduced aggregation (for comparison see also ESI, Fig. S9 and S10).

Gel composite preparation

Compositional optimization and dynamic crosslinking are critical to PIL-based gel performance for achieving high ionic conductivity and enabling simultaneous self-healing through reversible noncovalent interactions. In a typical synthesis, the multicomponent gel is prepared by first formulating a precursor mixture containing the IL-functionalized monomer (**M-IL**), the UPy-based monomer (**M-UPy**), ionic liquid (**IL**), lithium salt, and nanoparticles (for generating gel composites). The homogeneous mixture is subsequently polymerized *via* photopolymerization to yield a self-standing, transparent gel film (Fig. 3).[32]

In our previous investigation, formulations devoid of NPs included 1,6-hexanediol dimethacrylate as a covalent crosslinker.[32] Covalent crosslinker effectively enhanced the gel's stretchability, but it simultaneously reduced its ability to self-heal or be reprocessed due to the formation of permanent networks. In the present work, we eliminated the 1,6-hexanediol dimethacrylate crosslinker to promote dynamic and reversible interactions, compensating for the potential loss in mechanical strength by incorporating surface-modified nanofillers.

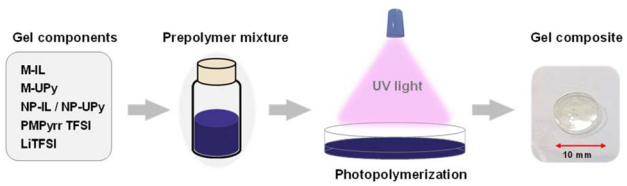

Fig. 3 Schematic representation of gel electrolyte preparation.

Our approach focused on introducing nanofillers while maintaining the other components constant, to understand the effect of nanoparticle incorporation prior to further optimization. The prepared compositions are summarized in Table 1. **G1** serves as the reference sample, containing the covalent crosslinker but no nanofillers. Formulations incorporating 5 and 10 wt% of **NP-IL** (**G2** and **G3**, respectively) exhibited a reduction in ionic conductivity from 1.1×10^{-4} S cm^{-1} (**G1**) to 9.5×10^{-5} S cm^{-1} (**G2**) and 6.9×10^{-5} S cm^{-1} (**G3**) at room temperature. Although **NP-IL** possesses abundant ionic liquid moieties on its surface, its presence likely restricts the mobility of the polymer chains and decreases the overall ionic conductivity. A similar trend was observed in mechanical testing (Fig. 4A): the reference gel **G1** showed the highest elongation at break, whereas **G2** and **G3** fractured at lower elongations. Subsequently, we prepared gel formulations without covalent crosslinkers but with additional nanofillers (keeping the molar ratio of **M-IL** and **M-UPy** constant). A comparison between **G2** (containing a covalent crosslinker) and its counterpart **G4** (without the covalent crosslinker) revealed a significant improvement in mechanical flexibility. Elongation at break increased from 146% (**G2**) to 466% (**G4**) – a more than threefold enhancement (Fig. 4B). Additionally, the tensile strength rose from 0.58 MPa to 0.83 MPa, indicating that the nanofillers contributed to reinforcement of the polymer network. Further increasing the **NP-IL** content slightly reduced the elongation at break to 386% (**G6**), suggesting that excessive filler loading may lead to reduced chain mobility.

A similar behavior was observed for composites containing **NP-UPy** (Fig. 4C). However, the incorporation of **NP-UPy** was limited to below 5 wt% as higher contents led to reduced dispersivity, forming non-transparent samples. This is presumably due to strong interparticle interactions, which promote aggregation. In contrast, **NP-IL** could be incorporated at higher concentrations as a result of improved dispersibility by IL-functionalized surfaces (better chemical compatibility with the ionic liquid-based polymer matrix). The ionic conductivity of the gel composites was characterized using broadband dielectric spectroscopy (BDS) over a temperature range of −20 to 70 °C (see ESI, Fig. S11–S18). In a typical measurement, the

Table 1 Gel composite compositions with varying contents of **NP-IL** and **NP-UPy** and their corresponding properties

Sample	Covalent crosslinker	Molar ratios			IL (wt%)	Li salt (wt%)	Nanofiller	Nanofiller amount (wt%)	Conductivity at RT (S cm^{-1})	Tensile strength (MPa)	Elongation at break (%)
		M-IL	**M-UPy**	C							
G1	+	10.4	8	1	48.7	16.3	—	—	1.1×10^{-4}	0.66	189
G2	+	10.4	8	1	46.3	15.4	**NP-IL**	5	9.5×10^{-5}	0.58	145
G3	+	10.4	8	1	43.5	14.6	**NP-IL**	10	6.9×10^{-5}	0.73	146
G4	–	10.4	8	0	46.3	15.4	**NP-IL**	5	2.2×10^{-4}	0.83	466
G5	–	10.4	8	0	43.5	14.6	**NP-IL**	10	1.2×10^{-4}	0.86	437
G6	–	10.4	8	0	41.4	13.8	**NP-IL**	15	8.7×10^{-5}	0.9	386
G7	–	10.4	8	0	46.3	15.4	**NP-UPy**	1	1.3×10^{-4}	0.87	483
G8	–	10.4	8	0	43.5	14.6	**NP-UPy**	5	1.8×10^{-4}	0.85	424

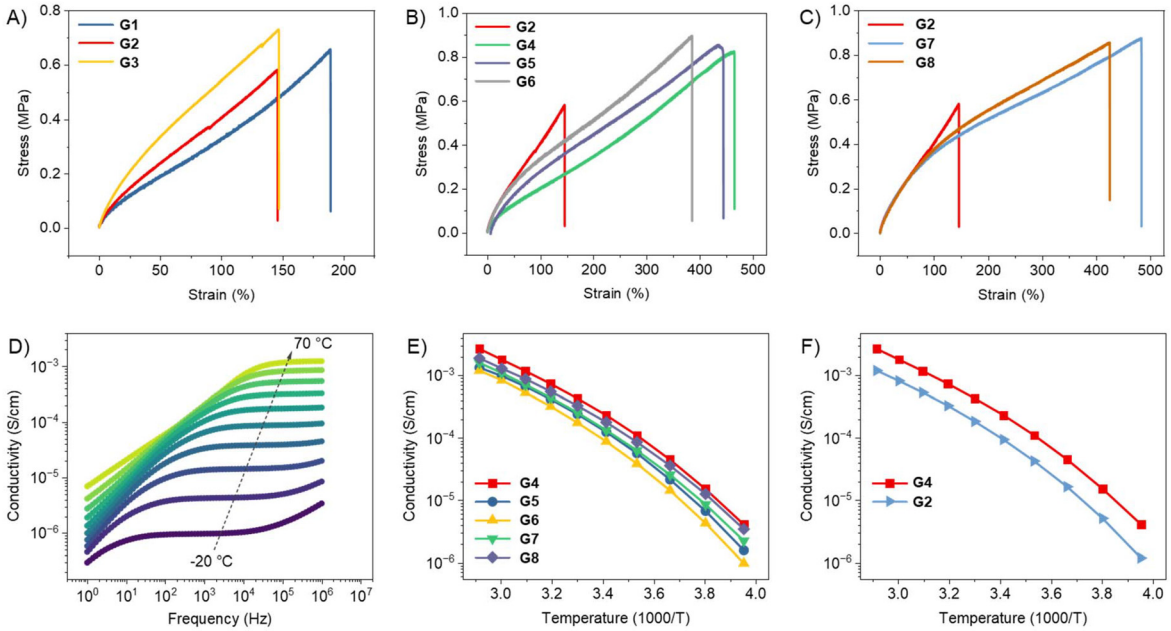

Fig. 4 Stress–strain curves of PIL gel composites (strain rate of 20 mm min^{-1}): (A) **G1–G3**, (B) **G2** and **G4–G6**, and (C) **G2**, **G7** and **G8**. (D) Frequency-dependent conductivity in the temperature range of −20 to 70 °C with 10 °C increments. Conductivity as a function of inverse temperature for (E) **G4–G8** and (F) **G4** *vs.* **G2**.

dielectric response was recorded across a frequency range of 10–10^7 Hz. The resulting frequency-dependent conductivity curves (Fig. 4D) exhibit a distinct plateau region at each temperature, from which the DC conductivity values were extracted. A significant increase in conductivity was observed with increasing temperatures, as expected. The temperature-dependent conductivity plots for the gel composites (Fig. 4E) display a nonlinear relationship, characteristic of polymer-based electrolytes. This behavior follows the Vogel–Tammann–Fulcher (VTF) model (ESI, Fig. S3),[44,45] which describes ion transport in polymeric systems and reflects the dynamic nature of the gel matrices. Among the studied samples, **G4** exhibited the highest conductivity values across the entire temperature range. With the incorporation of only 5 wt% **NP-IL**, **G4** achieved a maximum conductivity of 2.7 mS cm^{-1} at 70 °C. A comparison between **G4** and **G2** indicates that the removal of the covalent crosslinker and the addition of **NP-ILs** resulted in a more than two-fold improvement in conductivity across all temperatures (Fig. 4F). Furthermore, the ionic conductivity of the gel composites was evaluated after 12 months of storage in a glovebox and showed no significant change compared to the pristine material, confirming the good long-term stability of the prepared gel composites (ESI, Fig. S23).

In addition to ionic conductivity, the thermal and safety properties of the polymer electrolytes were evaluated. Thermogravimetric analysis (Fig. 5A) confirmed that the composites exhibited excellent thermal stability, with no significant weight loss up to 330 °C for **NP-IL**-containing formulations. In contrast, systems utilizing **NP-UPy** particles showed degradation onset above 250 °C, indicating a lower thermal stability limit for those materials. Another critical parameter

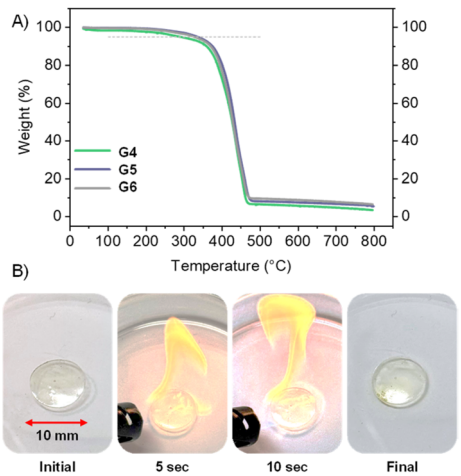

Fig. 5 (A) Thermogravimetric analysis of **G4–G6** and (B) flammability test of gel composites.

for electrolyte safety is flammability. As shown in Fig. 5B, the gel composites are entirely flame retardant. In a simple test, a direct flame was applied to the specimen for 10 seconds. The material neither ignited nor exhibited any visible degradation. These observations were further confirmed by UL 94 flammability tests, in which the material achieved a V-0 grading for a thickness of 1 mm (see ESI, Table S1 and Fig. S22), demonstrating its excellent flame retardancy and suitability for safe electrochemical applications.

The introduction of additional dynamic interactions (ionic interactions derived from **NP-IL** and supramolecular

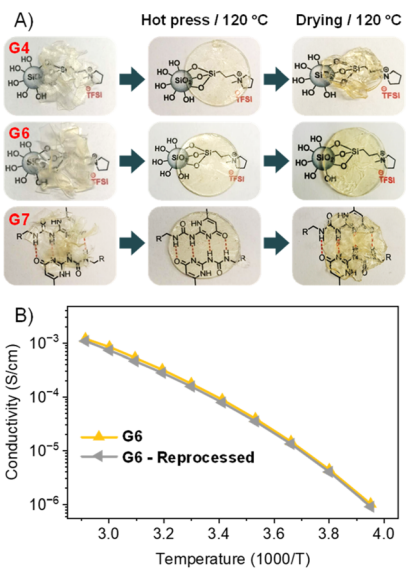

Fig. 6 (A) Reprocessing of **G4**, **G6** and **G7** *via* hot-pressing at 120 °C for 3 hours. (B) Conductivity as a function of temperature of **G6** before and after reprocessing.

hydrogen-bonding interactions contributed by **NP-UPy**) was expected to enhance the reprocessability of the gel composites. To evaluate this, broken gel fragments were placed into a mold and reprocessed using a hot-vacuum press at 120 °C for 3 hours. The results of this procedure are presented in Fig. 6A. Regardless of the type or amount of additional fillers, all composites exhibited complete recovery of their macroscopic shape, forming transparent, self-standing films after reprocessing. However, subsequent drying at 120 °C under vacuum for eliminating any residual moisture affected the dimensional stability. Gels containing higher contents of **NP-IL** demonstrated superior shape retention and structural integrity after drying, while those with lower **NP-IL** or **NP-UPy** content displayed noticeable deformation or shrinkage. To further verify the effectiveness of the reprocessing process, broadband dielectric spectroscopy measurements were performed on the reprocessed gels. As shown in Fig. 6B, the temperature-dependent conductivity of the reprocessed **G6** sample nearly overlapped with that of the pristine material, indicating that the ionic transport characteristics were fully restored. Thus, the dynamic crosslinking interactions enabled efficient reformation of the gel network without significant loss of electrochemical performance.

Conclusions

PIL-based gel composites were successfully prepared by incorporating surface-modified silica nanoparticles functionalized with either ionic liquid or multiple hydrogen bonds (ureidopyrimidinone) to embed reprocessability and dynamic properties into a solid electrolyte, reinforced by the nanoparticle-network. The covalent attachment of the hydrogen bonds to the nanoparticle surfaces was confirmed through various characterization techniques, including solid-state CP MAS ^{29}Si NMR spectroscopy, FT-IR, and thermogravimetric analysis. The introduction of these surface-modified nanoparticles significantly enhanced the dynamic behavior of the resulting gel composites. Specifically, samples demonstrated improved reprocessability and remarkable mechanical flexibility, achieving elongations at break of up to 460%. Notably, these mechanical properties were achieved solely through dynamic interactions, without the need for permanent covalent crosslinking. Furthermore, reprocessing of composites displayed high efficiency, completely recovering ionic conductivity. The gels additionally exhibited excellent ionic transport characteristics across a broad temperature range, achieving a conductivity of 2.2×10^{-4} S cm^{-1} at room temperature together with an outstanding thermal stability, with decomposition temperatures up to 330 °C. They were further inherently flame retardant, showing their potential for safe and durable applications in electrochemical and flexible devices. This allows the gel to be reshaped, repaired, or fully reprocessed without significant loss of performance. For recovery from used batteries, the battery would first undergo standard disassembly procedures, including removal of the casing, current collectors, and electrode stacks. Since the gel electrolyte is typically located within the separator or at the electrode–electrolyte interface, the electrode layers can be carefully separated mechanically. Through controlled solvent treatment or thermal activation of the dynamic bonds, the gel electrolyte can be detached from the electrodes and reprocessed into a new film or reshaped for reuse.

Author contributions

Conceptualization: A. M., Z. K. and W. H. B.; data curation: H. H., T. L. T., R. G. S. and Z. K.; formal analysis: H. H., R. G. S. and Z. K.; funding acquisition: A. M. and W. H. B.; investigation: H. H., T. L. T., R. G. S., S. K., H. R., A. M. and Z. K.; methodology: A. M., Z. K. and W. H. B.; project administration: A. M., Z. K. and W. H. B.; resources: A. M., Z. K. and W. H. B.; supervision: A. M., Z. K. and W. H. B.; validation: H. H., T. L. T., R. G. S. and Z. K.; visualization: H. H. and Z. K.; writing – original draft preparation: H. H., A. M., Z. K. and W. H. B.; writing – review and editing: H. H., A. M., Z. K. and W. H. B. All authors have read and agreed to the published version of the manuscript.

Conflicts of interest

There are no conflicts to declare.

Data availability

All original data are stored in our electronic labnotebook (E-lab), where they can be retrieved on demand. Organization

of these data inside the system follows the rules of the DFG (German Research Foundation). Access can be granted on request but cannot be provided by an open link, to secure other data inside the system. We provide all data on ^{1}H-NMR, ^{13}C-NMR, tensile testing, CP-MAS, TGA, FT-IR, TEM and BDS electronically on demand.

Supplementary information (SI) is available. See DOI: https://doi.org/10.1039/d6py00098c.

Acknowledgements

The authors acknowledge financial support from the Just Transition Center (JTC) and the DFG project BI1337/18-1 (Nr 551070679). The authors thank Alexey Krushelnitsky (Institute of Physics, Martin-Luther-University Halle-Wittenberg) for performing the solid-state NMR measurements and Annett Quetschke (Institute of Chemistry, Martin-Luther-University Halle-Wittenberg) for performing the TGA-MS measurements.

References

1 N. Nasajpour-Esfahani, H. Garmestani, M. Bagheritabar, D. J. Jasim, D. Toghraie, S. Dadkhah and H. Firoozeh, *Renewable Sustainable Energy Rev.*, 2024, **203**, 114783.
2 M. Li, J. Lu, Z. Chen and K. Amine, *Adv. Mater.*, 2018, **30**, 1800561.
3 J. Jaguemont and F. Bardé, *Appl. Therm. Eng.*, 2023, **231**, 121014.
4 Y. Alex, N. Divakaran, P. Srinivasan, U. T. Uthappa, S. Mubarak, M. Al-Harthi and D. Dhamodharan, *J. Energy Storage*, 2026, **141**, 119317.
5 M. Rezaei, A. Nekahi, A. Kumar M R, A. Nizami, X. Li, S. Deng, J. Nanda and K. Zaghib, *J. Power Sources*, 2025, **630**, 236157.
6 A. Marinow, Z. Katcharava and W. H. Binder, *Polymers*, 2023, **15**, 1145.
7 M. Li, C. Wang, Z. Chen, K. Xu and J. Lu, *Chem. Rev.*, 2020, **120**, 6783–6819.
8 T. Zhou, C. Gui, L. Sun, Y. Hu, H. Lyu, Z. Wang, Z. Song and G. Yu, *Chem. Rev.*, 2023, **123**, 12170–12253.
9 X. Ma, J. Yu, Y. Hu, J. Texter and F. Yan, *Ind. Chem. Mater.*, 2023, **1**, 39–59.
10 L. Liang, X. Chen, W. Yuan, H. Chen, H. Liao and Y. Zhang, *ACS Appl. Mater. Interfaces*, 2021, **13**, 25410–25420.
11 T. Zhou, X. Gao, B. Dong, N. Sun and L. Zheng, *J. Mater. Chem. A*, 2016, **4**, 1112–1118.
12 X. Wei, T. Lin, J. Gao, Y. Hu, Z. Zhang, J. Peng, J. Li and M. Zhai, *ACS Appl. Mater. Interfaces*, 2024, **16**, 12586–12598.
13 B. Yang, G. Yang, Y.-M. Zhang and S. X.-A. Zhang, *J. Mater. Chem. C*, 2021, **9**, 4730–4741.
14 W. Zhou, M. Zhang, X. Kong, W. Huang and Q. Zhang, *Adv. Sci.*, 2021, **8**, 2004490.
15 Z. Katcharava, A. Marinow and W. H. Binder, *Chem. Commun.*, 2025, **61**, 3250–3270.
16 M. Guerre, C. Taplan, J. M. Winne and F. E. Du Prez, *Chem. Sci.*, 2020, **11**, 4855–4870.
17 V. Schenk, K. Labastie, M. Destarac, P. Olivier and M. Guerre, *Mater. Adv.*, 2022, **3**, 8012–8029.
18 K. Ahuja, P. Singh, N. Banerjee, S. Rana, G. J. Yun, F. Ahmad and M. Jamil, *J. Energy Storage*, 2025, **126**, 117077.
19 P. Fan, H. Liu, V. Marosz, N. T. Samuels, S. L. Suib, L. Sun and L. Liao, *Adv. Funct. Mater.*, 2021, **31**, 2101380.
20 S. Tang, W. Guo and Y. Fu, *Adv. Energy Mater.*, 2021, **11**, 2000802.
21 S. Liu, W. Liu, D. Ba, Y. Zhao, Y. Ye, Y. Li and J. Liu, *Adv. Mater.*, 2023, **35**, 2110423.
22 S.-Y. Zhang, Q. Zhuang, M. Zhang, H. Wang, Z. Gao, J.-K. Sun and J. Yuan, *Chem. Soc. Rev.*, 2020, **49**, 1726–1755.
23 B. Zhou, Y. H. Jo, R. Wang, D. He, X. Zhou, X. Xie and Z. Xue, *J. Mater. Chem. A*, 2019, **7**, 10354–10362.
24 Y. Lu, K. Korf, Y. Kambe, Z. Tu and L. A. Archer, *Angew. Chem., Int. Ed.*, 2014, **53**, 488–492.
25 B. Zhou, D. He, J. Hu, Y. Ye, H. Peng, X. Zhou, X. Xie and Z. Xue, *J. Mater. Chem. A*, 2018, **6**, 11725–11733.
26 X. Chen, L. Yi, C. Zou, J. Liu, J. Yu, Z. Zang, X. Tao, Z. Luo, X. Guo, G. Chen, B. Chang, Y. Shen and X. Wang, *ACS Appl. Energy Mater.*, 2022, **5**, 5267–5276.
27 Y. H. Jo, B. Zhou, K. Jiang, S. Li, C. Zuo, H. Gan, D. He, X. Zhou and Z. Xue, *Polym. Chem.*, 2019, **10**, 6561–6569.
28 Q. Dou, L. Liu, B. Yang, J. Lang and X. Yan, *Nat. Commun.*, 2017, **8**, 2188.
29 Z. Katcharava, A. Marinow, R. Bhandary and W. H. Binder, *Nanomaterials*, 2022, **12**, 1859.
30 H. Niu, M. Ding, N. Zhang, X. Guo, P. Guan and X. Hu, *ChemElectroChem*, 2023, **10**, e202201015.
31 H. Qi, Y. Ren, S. Guo, Y. Wang, S. Li, Y. Hu and F. Yan, *ACS Appl. Mater. Interfaces*, 2020, **12**, 591–600.
32 Z. Katcharava, T. E. Orlamünde, L. T. Tema, H. Hong, M. Beiner, B. Iliev, A. Marinow and W. H. Binder, *Adv. Funct. Mater.*, 2024, **34**, 2403487.
33 C. Li, R. Bhandary, A. Marinow, D. Ivanov, M. Du, R. Androsch and W. H. Binder, *Polymers*, 2022, **14**, 4090.
34 B. J. B. Folmer, R. P. Sijbesma, R. M. Versteegen, J. A. J. van der Rijt and E. W. Meijer, *Adv. Mater.*, 2000, **12**, 874–878.
35 G. Engelhardt and H. Jancke, *Polym. Bull.*, 1981, **5**, 577–584.
36 I. S. Protsak, Y. M. Morozov, W. Dong, Z. Le, D. Zhang and I. M. Henderson, *Nanoscale Res. Lett.*, 2019, **14**, 160.
37 T. Sen and I. J. Bruce, *Sci. Rep.*, 2012, **2**, 564.
38 L. Garcia-Quintana, F. Chen, N. Ortiz-Vitoriano, Y. Zhang, L. A. O'Dell, D. R. MacFarlane, M. Forsyth, A. M. Bond, P. C. Howlett and C. Pozo-Gonzalo, *Batteries Supercaps*, 2021, **4**, 513–521.
39 I. Rey, P. Johansson, J. Lindgren, J. C. Lassègues, J. Grondin and L. Servant, *J. Phys. Chem. A*, 1998, **102**, 3249–3258.

40 R. Suriano, L. Brambilla, M. Tommasini and S. Turri, *Polym. Adv. Technol.*, 2018, **29**, 2899–2908.
41 W. P. J. Appel, G. Portale, E. Wisse, P. Y. W. Dankers and E. W. Meijer, *Macromolecules*, 2011, **44**, 6776–6784.
42 Z. Wang, Y. Ding and J. Wang, *Nanomaterials*, 2019, **9**, 1397.
43 L. T. Zhuravlev, *Langmuir*, 1987, **3**, 316–318.
44 K. M. Diederichsen, H. G. Buss and B. D. McCloskey, *Macromolecules*, 2017, **50**, 3831–3840.
45 S. B. Aziz, T. J. Woo, M. F. Z. Kadir and H. M. Ahmed, *J. Sci.: Adv. Mater. Devices*, 2018, **3**, 1–17.